nanomaterials

MDPI

Article

Facile Construction and Fabrication of a Superhydrophobic and Super Oleophilic Stainless Steel Mesh for Separation of Water and Oil

Yinyu Sun, Zhongcheng Ke *, Caiyun Shen, Qing Wei, Ruikang Sun, Wei Yang and Zihan Yin

School of Chemistry and Chemical Engineering, Huangshan University, Huangshan 245021, China; yysun_hsu@163.com (Y.S.); ascy8843@163.com (C.S.); wq19105591009@163.com (Q.W.); sunruikangjnu@163.com (R.S.); myxhjsn996320687@163.com (W.Y.); yzh20030201@163.com (Z.Y.)
* Correspondence: xiaoke1020@126.com; Tel.: +86-139-5599-7920

Abstract: The fluoride-free fabrication of superhydrophobic materials for the separation of oil/water mixtures has received widespread attention because of frequent offshore oil exploration and chemical leakage. In recent years, oil/water separation materials, based on metal meshes, have drawn much attention, with significant advantages in terms of their high mechanical strength, easy availability, and long durability. However, it is still challenging to prepare superhydrophobic metal meshes with high-separation capacity, low costs, and high recyclability for dealing with oil–water separation. In this work, a superhydrophobic and super oleophilic stainless steel mesh (SSM) was successfully prepared by anchoring Fe_2O_3 nanoclusters (Fe_2O_3-NCs) on SSM via the in-situ flame synthesis method and followed by further modification with octadecyltrimethoxysilane (OTS). The as-prepared SSM with Fe_2O_3-NCs and OTS (OTS@Fe_2O_3-NCs@SSM) was confirmed by a field emission scanning electron microscope (FESEM), transmission electron microscope (TEM), energy dispersive spectrometer (EDS), X-ray photoelectron spectrometer (XPS), and X-ray diffractometer (XRD). The oil–water separation capacity of the sample was also measured. The results show that the interlaced and dense Fe_2O_3-NCs, composed of Fe_2O_3 nanoparticles, were uniformly coated on the surface of the SSM after the immerging-burning process. Additionally, a compact self-assembled OTS layer with low surface energy is coated on the surface of Fe_2O_3-NCs@SSM, leading to the formation of OTS@Fe_2O_3-NCs@SSM. The prepared OTS@Fe_2O_3-NCs@SSM shows excellent superhydrophobicity, with a water static contact angle of 151.3°. The separation efficiencies of OTS@Fe_2O_3-NCs@SSM for the mixtures of oil/water are all above 98.5%, except for corn oil/water (97.5%) because of its high viscosity. Moreover, the modified SSM exhibits excellent stability and recyclability. This work provides a facile approach for the preparation of superhydrophobic and super oleophilic metal meshes, which will lead to advancements in their large-scale applications on separating oil/water mixtures.

Keywords: stainless steel mesh; Fe_2O_3 nanoclusters; octadecyltrimethoxysilane; oil–water separation

Citation: Sun, Y.; Ke, Z.; Shen, C.; Wei, Q.; Sun, R.; Yang, W.; Yin, Z. Facile Construction and Fabrication of a Superhydrophobic and Super Oleophilic Stainless Steel Mesh for Separation of Water and Oil. *Nanomaterials* **2022**, *12*, 1661. https://doi.org/10.3390/nano12101661

Academic Editors: John Vakros, Evroula Hapeshi, Catia Cannilla, Giuseppe Bonura and Marco Stoller

Received: 25 April 2022
Accepted: 11 May 2022
Published: 13 May 2022

1. Introduction

The cost-effective separation strategies of oil/water mixtures have become a hot topic due to the frequent occurrences of water pollution issues, such as organic wastewater emissions, chemical leaks, and crude oil spills [1–4]. To date, a series of materials, including carbon aerogels [5–8], cotton fabrics [9–12], foams [13–15], and sponges [16–19], have been explored, owing to the excellent hydrophobicity and high separation capacity. However, some materials are difficult to use in large-scale applications because of the complicated and high-cost separation process, secondary contamination, or poor recyclability. From the perspective of application, it is necessary to develop a more efficient, facile, and low-cost method to achieve the separation of water and oil.

Over the past few years, oil/water separation materials, based on metal meshes [20–22], especially stainless steel meshes (SSM) [23–26], have drawn much attention, with significant

advantages in terms of their high mechanical strength, easy availability, and long durability. The preparation of superhydrophobic mesh is mainly based on surface modification by changing the chemical composition or the microscopic geometry of the surface [27–30]. For example, Jiang et al. first prepared a superhydrophobic mesh with high oil–water separation efficiency via surface modification with polytetrafluoroethylene [31]. Chen et al. provided a facile approach for the preparation of oil–water separation material via the coating of the reduced graphene oxide on mesh [32]. Fu and co-workers prepared a robust superhydrophobic and super oleophilic material by loading hierarchical-layer nanospheres on the surface of metal mesh [33]. Liang et al. developed a co-precipitation strategy to prepare superhydrophobic materials by growing hierarchical micro-nanostructures of CeO_2 on the Cu mesh, followed by further modification with stearic acid [21]. Wang et al. reported that a superhydrophobic mesh was prepared via the coating of micro/nanostructured $Co(OH)_2$ on the mesh, followed by modification with hexadecyltrimethoxysilane [27]. Based on the aforementioned previous research, the rough surface caused by the loading of nanoparticles can greatly increase the surface area of the substrate. Furthermore, the superhydrophobic surface is usually achieved by surface modification with a low-surface-energy material. Nevertheless, most methods of preparing the oil/water separation material are usually costly, such as expensive equipment or devices, complex synthesis steps, toxic reagents, or by-products. Therefore, it is necessary to develop a facile strategy to prepare superhydrophobic SSM with high separation capacity, low costs, and high recyclability for dealing with oil/water separation.

In this work, an SSM with a superhydrophobic and super oleophilic surface was successfully prepared by anchoring Fe_2O_3 nanoclusters (Fe_2O_3-NCs) by the in-situ flame synthesis method and then modified with octadecyltrimethoxysilane (OTS). The SSM with OTS and Fe_2O_3-NCs (OTS@Fe_2O_3-NCs@SSM) was characterized with a field emission scanning electron microscope (FESEM), energy dispersive X-ray spectrometer (EDS), X-ray photoelectron spectrometer (XPS), and X-ray diffractometer (XRD). Additionally, the oil–water separation capacity and recyclability of the samples were also examined.

2. Materials and Methods

2.1. Materials

Ferric acetylacetonate ($C_{15}H_{21}FeO_6$, 99%), absolute ethanol, and OTS were purchased from Macklin biochemical technology Co., Ltd., China (Shanghai, China). The commercial SSM of 400 meshes was purchased from Taobao (Changzhou, China). The SSM with a size of 5 × 5 cm was ultrasonically cleaned in ethanol for 1 h and then dried at 80 °C in air for 5 h. Distilled water was used in all the experiments.

2.2. Preparation of OTS@Fe_2O_3-NCs@SSM

Firstly, SSM was dipped into a solution containing 100 mL of ethanol and 2.2 g of $C_{15}H_{21}FeO_6$ for 5 s to get SSM filled with the solution and followed by burning in air. This process was repeated 40 times to ensure the loading of Fe_2O_3-NCs on SSM (Fe_2O_3-NCs@SSM). The as-obtained Fe_2O_3-NCs@SSM was cleaned with deionized water and dried at 80 °C in air for 3 h. Secondly, 0.5 mL of OTS was ultrasonically dissolved in 400 mL of distilled water for 1 h. Subsequently, Fe_2O_3-NCs@SSM was added into the aforementioned aqueous emulsion and left for 24 h. Finally, the as-obtained OTS@Fe_2O_3-NCs@SSM was cleaned with deionized water and dried at 80 °C in air for 5 h.

2.3. Physical Characterizations

The morphologies were observed using FESEM (Gemini 500, Zeiss, Oberkochen, Germany) and TEM (Tecnai G^2 F20, FEI, Ames, IA, USA). The surface elemental composition and distribution were determined by EDS (X-Max^N 80, Oxford, UK) and XPS (ESCALAB 250Xi, Thermo Fisher, Waltham, MA, USA). X-ray diffraction patterns were obtained by XRD equipped with a Cu Kα radiation source (D8 Advance, Bruker, Karlsruher, Germany). The water static contact angle was measured at room temperature via a

contact angle meter (DSA100, KRUSS, Hamburg, Germany). Zeta potential values were obtained using a solid zeta potential instrument (SurPass, Anton Paar, Graz, Austria) and nanoparticle size potentiometer (Nano ZS90, Malvern, Malvern, UK).

2.4. Oil–Water Separation and Recyclability Tests

In the oil/water separation test, the immiscible mixtures of water and oil or organic solvents in a 1:1 volume ratio were used. The mixtures were poured onto OTS@Fe_2O_3-NCs@SSM, which was fixed in the homemade device. The oil–water separation efficiency T was calculated by $(V_2/V_1) \times 100$, where V_1 and V_2 were the volume of water before and after separation, respectively. In the recyclability test, the separation process of the samples was repeated. After each cycle, the used samples were cleaned with ethanol and dried at 80 °C in air for 3 h.

3. Results and Discussion

3.1. Characterization

Figure 1 presents the schematic illustration of the controllable constructing process of OTS@Fe_2O_3-NCs@SSM via a simple and facile two-step strategy. Firstly, SSM wetted by the solution containing ethanol and $C_{15}H_{21}FeO_6$ was taken out and burned in air. In this immerging-burning process, absolute ethanol was not only used as a solvent to dissolve $C_{15}H_{21}FeO_6$, but also made $C_{15}H_{21}FeO_6$ sufficient for burning in air. In the meantime, hydrocarbon moieties and Fe atoms decomposed by $C_{15}H_{21}FeO_6$ at high temperatures acted as a source of carbon atoms and catalyst, respectively [34,35]. The hydrocarbon moieties were coated on Fe atoms to form an Fe–C bond [36]. Fe_2O_3-NCs nanoparticles were constantly deposited on the carbon precipitates to grow Fe_2O_3-NCs on the surface of SSM after repeating 40 times for the immerging-burning process. The immobilization of Fe_2O_3-NCs on the surface of SSM is not only beneficial to enhance the surface roughness of SSM, but can also effectively improve the adhesion between hydrophobic components and SSM. Secondly, Fe_2O_3-NCs@SSM was added into the OTS aqueous emulsion, leading to the formation of OTS@Fe_2O_3-NCs@SSM. In particular, it needs to be mentioned that the growing of Fe_2O_3-NCs on SSM after immerging-burning treatment is beneficial to the coating of OTS on the surface of Fe_2O_3-NCs@SSM, which will enhance the superhydrophobic property of the material. Additionally, OTS can be used to grow a compact and self-assembled monolayer with low surface energy on the surface of Fe_2O_3-NCs@SSM, leading to an improvement in the hydrophobicity of the sample [37,38].

The surface morphology of samples was demonstrated by FESEM and TEM images. As shown in Figure 2a,d, the typical FESEM images of the untreated SSM exhibit a smooth surface, with a diameter of ca. 34 μm, which is used as the substrate to adsorb $C_{15}H_{21}FeO_6$. After the dipping–burning process, the interlaced and dense Fe_2O_3-NCs are uniformly coated on the surface of the SSM, with a diameter of ca. 40 μm (Figure 2b,e). The thickness of the Fe_2O_3-NCs layer was found to be ca. 3 μm, based on the difference in diameter between SSM and Fe_2O_3-NCs@SSM. The TEM image (Figure 3) clearly confirms that Fe_2O_3-NCs are composed of Fe_2O_3 nanoparticles. It is notable that Fe_2O_3-NCs not only provides the larger surface area for the loading of OTS, but also effectively enhances the adhesion between OTS and SSM. After modification, a dense self-assembled OTS layer is coated on the surface of Fe_2O_3-NCs@SSM, leading to the formation of OTS@Fe_2O_3-NCs@SSM (Figure 2c,f).

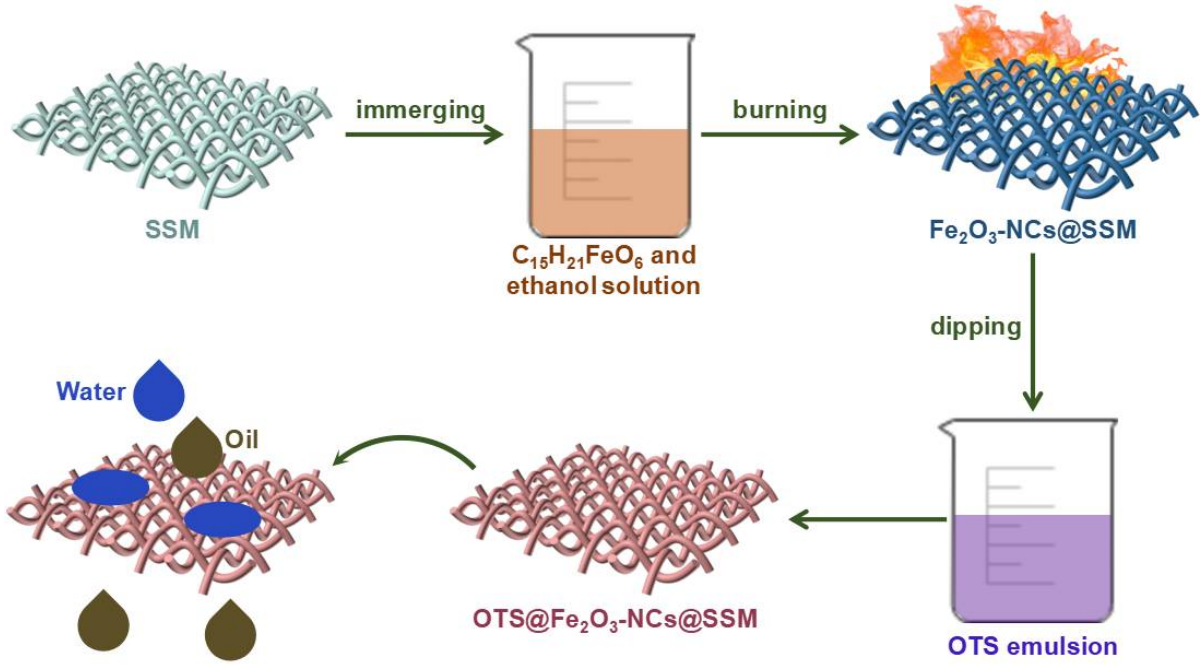

Figure 1. Schematic illustration of the preparation of OTS@Fe_2O_3-NCs@SSM.

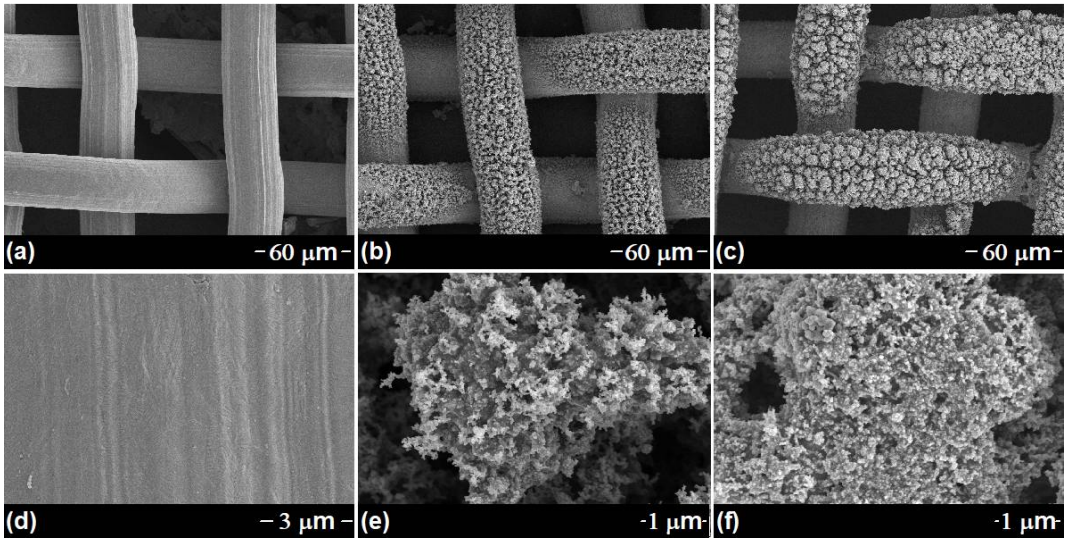

Figure 2. FESEM images of SSM (**a**,**d**), Fe_2O_3-NCs@SSM (**b**,**e**), OTS@Fe_2O_3-NCs@SSM (**c**,**f**).

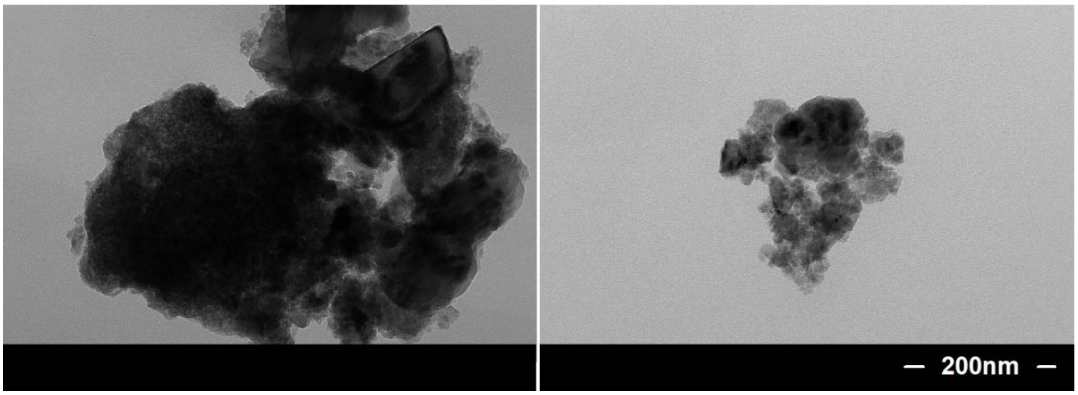

Figure 3. TEM image of Fe_2O_3-NCs.

The chemical compositions of samples were tested by EDS and XPS. The SEM-based EDS elemental analysis results (Figures S1–S3) revealed that the elemental content of O on Fe_2O_3-NCs@SSM was obviously increased, compared with SSM, due to the formation of Fe_2O_3-NCs on the surface of SSM after the immerging-burning process. It is worth noting that the proportion of Si element on SSM and Fe_2O_3-NCs@SSM are 0.31 and 0%, respectively. These results suggest that the Si element was undetected on the surface of Fe_2O_3-NCs@SSM because of the interlaced and dense Fe_2O_3-NCs coated on SSM. As described in Figure S3 and Figure 4, the elemental distribution of Si components on OTS@Fe_2O_3-NCs@SSM can verify that the hydrophobic components of OTS are successfully coated on the substrate. As shown in Figure 5a, the surface XPS results of SSM verify the existence of C (284.6 eV), O (530.6 eV), and Fe (711.2 eV) elements [30]. In addition, the Si 2s and Si 2p signal peaks are detected on the surface of SSM, which is consistent with the EDS results (Figure S1). The absence of Si 2s peak in the XPS results of Fe_2O_3-NCs@SSM may be caused by the coating of Fe_2O_3-NCs on SSM, which agrees well with the EDS results shown in Figure S2. The Si 2s and Si 2p peaks are present in the XPS results of OTS@Fe_2O_3-NCs@SSM, which originated from OTS [39]. These XPS results can further confirm the successful preparation of Fe_2O_3-NCs and OTS on the surface of SSM.

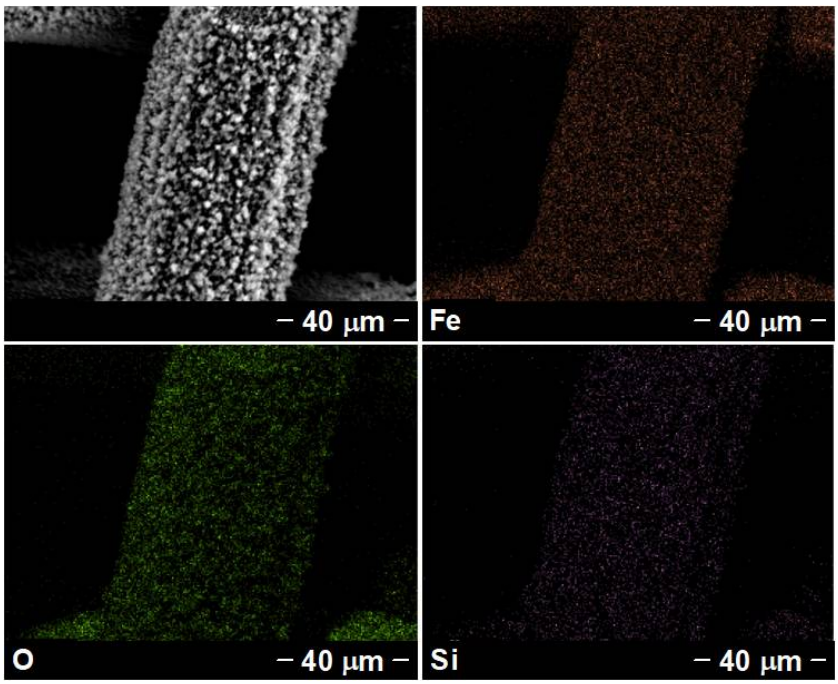

Figure 4. Images of OTS@Fe_2O_3-NCs@SSM on EDS elemental mappings.

As shown in Figure 5b, the crystal phases of SSM, Fe_2O_3-NCs@SSM, and OTS@Fe_2O_3-NCs@SSM were analyzed by XRD patterns. The XRD patterns of the samples have two characteristic peaks at 44.0 and 51.1°, which are assigned to the (111) and (200) lattice planes of SSM, respectively [30]. In addition, the diffraction patterns of Fe_2O_3-NCs@SSM exhibit four characteristic peaks, corresponding to the (104), (110), (024), and (214) lattice planes of Fe_2O_3 nanoparticles at 33.2, 35.6, 49.5, and 62.4°, respectively [37]. This result can further confirm the successful preparation of Fe_2O_3-NCs on the surface of SSM. No obvious characteristic diffraction peaks for OTS can be detected due to its poor crystallinity. As can be seen in Table S1, the zeta potentials of the samples were measured. The charge of SSM is −63.25 mV in 1 mM KCl aqueous solution at pH = 7, which is consistent with previous studies [40,41]. After the immerging-burning process, the surface charge of Fe_2O_3-NCs@SSM increases to −45.09 mV due to the coating of Fe_2O_3-NCs with a zeta potential value of −14.17 mV. Moreover, the zeta potential of OTS@Fe_2O_3-NCs@SSM is still negatively charged with a value of −27.83 mV, which can be attributed to the further

loading of OTS, with a zeta potential value of −26.10 mV. These results suggest that Fe_2O_3-NCs and OTS are successfully immobilized on the surface of SSM.

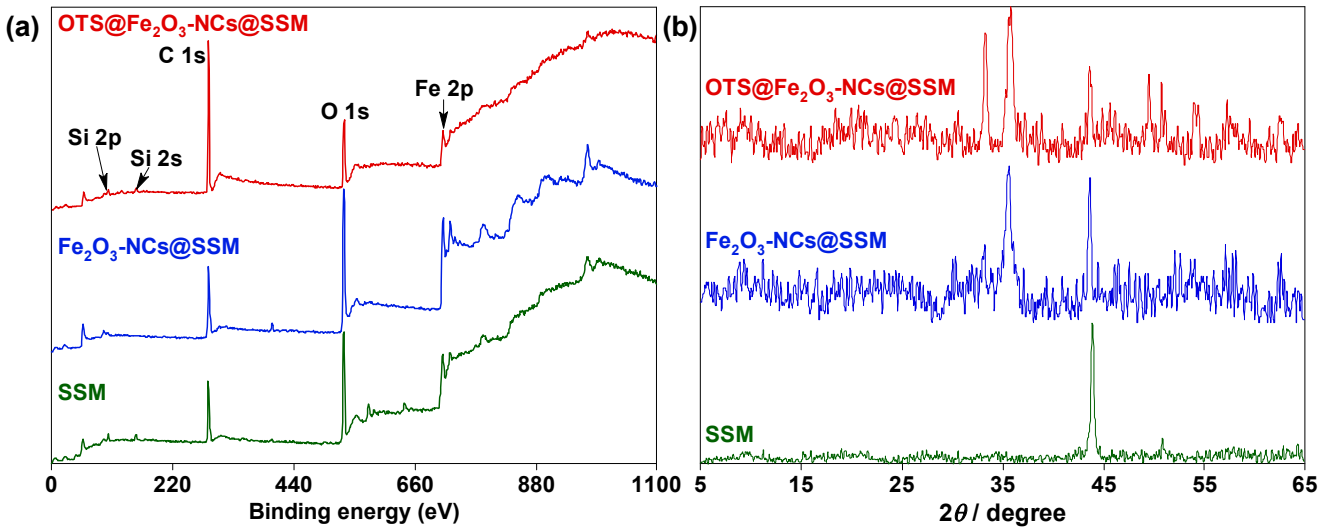

Figure 5. (**a**) XPS analysis of SSM, Fe_2O_3-NCs@SSM, and OTS@Fe_2O_3-NCs@SSM. (**b**) XRD patterns of SSM, Fe_2O_3-NCs@SSM, and OTS@Fe_2O_3-NCs-NCs@SSM.

3.2. Superhydrophobic Performance

The surface hydrophobicity of the sample is very important to support potential practical applications. As depicted in Figure 6a, water and methyl blue solution droplets were prevented from penetrating through OTS@Fe_2O_3-NCs@SSM, exhibiting excellent hydrophobic properties. Interestingly, a water column ejected from a syringe and bouncing off the superhydrophobic surface of OTS@Fe_2O_3-NCs@SSM, indicating that the modified SSM has an ultralow contact-angle hysteresis (Figure 6b). To further evaluate the hydrophobicity of the samples, the floating test and the water static contact-angle test were carried out. As shown in Figure 6c, both SSM and Fe_2O_3-NCs@SSM sink to the bottom of water. However, OTS@Fe_2O_3-NCs@SSM can float on water and pick it up without water droplets. This result indicates that OTS@Fe_2O_3-NCs@SSM has better hydrophobicity than SSM and Fe_2O_3-NCs@SSM. As can be seen in Figure 6d–f, the water static contact angle of the samples was observed. The original SSM exhibits a hydrophilic property with a water static contact angle of ca. 116.5° (Figure 6d). The water static contact angle of Fe_2O_3-NCs@SSM is ca. 0° (Figure 6e). This result suggests that the hydrophilic component of Fe_2O_3-NCs changes the surface hydrophobicity of SSM. After modification, OTS@Fe_2O_3-NCs@SSM shows extreme superhydrophobic surface with a water static contact angle of 151.3° because of the uniform coating of the hydrophobic component of OTS on Fe_2O_3-NCs@SSM (Figure 6f). The preparation of superhydrophobic SSM can be explained by changing the microscopic geometry and the surface energy. Firstly, the rough surface caused by the formation of Fe_2O_3-NCs can retain more air beneath the water droplets, effectively reducing the solid–liquid contact area. Furthermore, OTS, a typical low-surface-energy material, is used to modify the surface property of Fe_2O_3-NCs@SSM, leading to enhanced hydrophobicity.

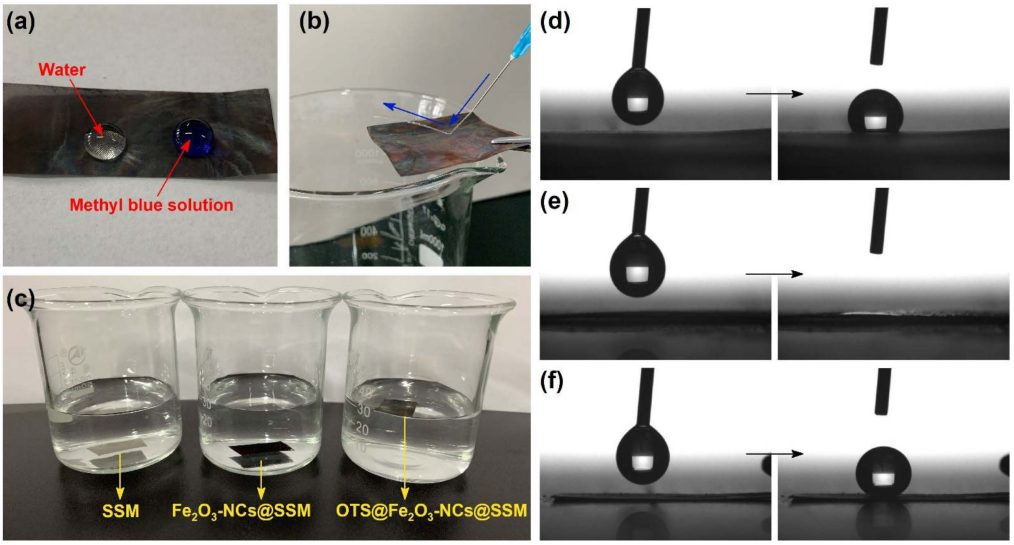

Figure 6. (**a**) Water and methyl blue droplets on the top of OTS@Fe_2O_3-NCs@SSM. (**b**) The water column reflects image on the surface of OTS@Fe_2O_3-NCs @SSM. (**c**) The floating test on water of the samples. (**d**–**f**) The water static contact-angle measurement of SSM, Fe_2O_3-NCs@SSM, and OTS@Fe_2O_3-NCs @SSM.

To ensure a better evaluation for the superhydrophobic behavior of the samples, the oil–water separation performance was tested. As shown in Figure 7, dichloromethane and water were dyed with oil red O and methyl blue, respectively. Subsequently, the mixtures were poured into the homemade gravity-driven separation device through OTS@Fe_2O_3-NCs@SSM. It was found that dichloromethane can quickly permeate through OTS@Fe_2O_3-NCs@SSM through the driving force of gravity and water retained on the top side of the modified mesh. The prepared OTS@Fe_2O_3-NCs@SSM has excellent performance to separate the oil/water mixtures due to the superhydrophobic and super oleophilic surfaces.

As depicted in Figure 8a, the oil–water separation efficiency was evaluated by the homemade separation device. The separation efficiencies of OTS@Fe_2O_3-NCs@SSM for the mixtures of petroleum toluene/water, n-octane/water, gasoline/water, n-hexane/water, chloroform/water, dichloromethane/water, and cyclohexane/water were all above 98.5%, except for corn oil/water (97.5%), because of its high viscosity. These data suggest that the prepared superhydrophobic SSM can be used as an ideal material to efficiently separate an oil/water mixture. As can be seen from the data in Table 1, the modified SSM shows higher separation efficiency than many previously reported meshes [22,24,33,42–46]. Although the separation efficiency of OTS@Fe_2O_3-NCs@SSM is still lower than that of those reported materials [21,27,32], the preparation method of OTS@Fe_2O_3-NCs@SSM is more facile, time saving, and economical. Therefore, OTS@Fe_2O_3-NCs@SSM is a cost-effective and promising material for oil/water separation. In addition, the oil–water separation materials should be easily cleaned and recycled in terms of the practical applications. The recycled experiments of the superhydrophobic and super oleophilic OTS@Fe_2O_3-NCs@SSM were also investigated (Figure 8b). The separation efficiency of the samples for the n-hexane/water mixture could be maintained above 98.6% after 10 cycles of separation, indicating the excellent reusability of the samples. In addition, data analysis of group 10 and group 0 shows that the p value is greater than 0.05, suggesting that the separation efficiency of the two groups is not significantly different. This result suggests that the immobilization of Fe_2O_3-NCs on the surface of SSM can effectively improve the adhesion between hydrophobic components and SSM and enhance the reusability of the material.

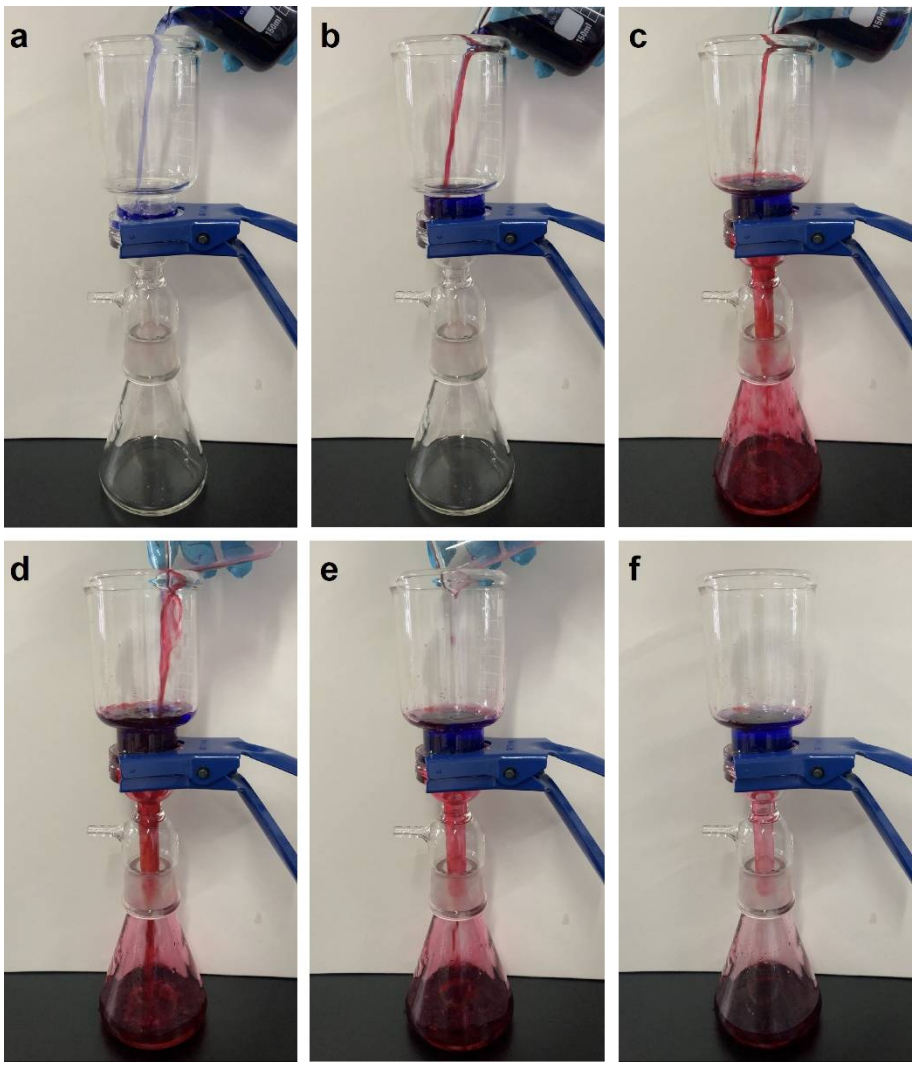

Figure 7. (**a**–**f**) Oil–water separation process of OTS@Fe_2O_3-NCs@SSM (water dyed with methyl blue and dichloromethane dyed with Oil red O).

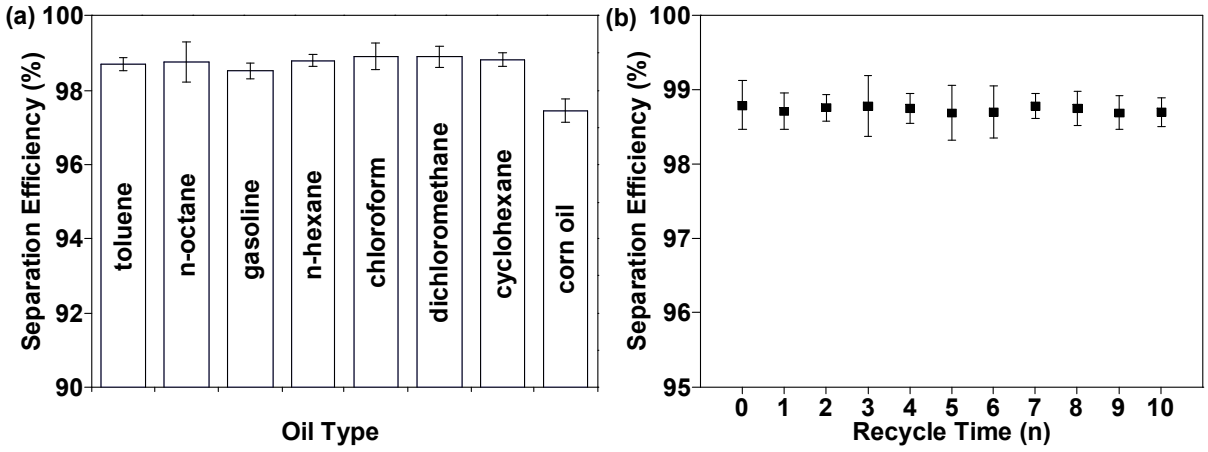

Figure 8. (**a**) Oil/water separation efficiencies of OTS@Fe_2O_3-NCs@SSM for oil or organic solvents. (**b**) Separation efficiency for the n-hexane/water mixture after 10 cycles.

Table 1. Comparison of various meshes for oil/water separation.

Matrix	Modified Materials	Method	Separation Efficiency (%)	Ref.
wire mesh	Graphene oxide	O_2 plasma and thermal annealing	>98	[32]
Cu mesh	1-dodecanethiol	Immersion and modification	>96	[22]
Cu Mesh	Lauric acid	Electrodeposition and modification	>93	[40]
Cu mesh	Na_2SiO_3 + Al_2O_3	Self-assemble	>95	[41]
Cu mesh	Stearic acid	Co-precipitation and modification	>99	[21]
SSM	Phytic acid and vinyltriethoxysilane	Immersion	>90	[33]
SSM	Natural flake mica	Hydrothermal synthesis and electrodeposition	>90	[42]
SSM	—	Laser ablation	>96	[24]
SSM	Hexadecyltrimethoxysilane	Pulse electrodeposition and modification	>99	[27]
SSM	TiO_2 nanofibers	Hydrothermal synthesis and spray deposition	>90	[43]
SSM	Glass particles	Laser texturing	>96	[44]
SSM	Fe_2O_3-NCs and OTS	Flame synthesis and modification	>97	This work

4. Conclusions

In summary, a robust and stable superhydrophobic and super oleophilic SSM was fabricated successfully by anchoring Fe_2O_3-NCs on SSM via the in-situ flame synthesis method and followed by further modification with OTS. The characterization results indicate that the preparation of Fe_2O_3-NCs, composed of Fe_2O_3 nanoparticles on the surface of SSM, is not only beneficial to enhance the surface roughness of SSM, but can also effectively improve the adhesion between hydrophobic components and SSM. In addition, the coating of OTS with low surface energy endows SSM with excellent superhydrophobicity, as well as super oleophilicity, with a water static contact angle of 151.3°. Moreover, the prepared OTS@Fe_2O_3-NCs@SSM exhibits excellent oil–water separation efficiency for a series of oil and water mixtures. It is important to note that the modified SSM shows good stability and reusability after 10 cycles. Therefore, this work provides an intriguing methodology for coating nanostructures on metal substrates, which will lead to a new perspective on separating oil/water mixtures.

Supplementary Materials: The following supporting information can be downloaded at: https://www.mdpi.com/article/10.3390/nano12101661/s1, Figure S1: Images of SSM on EDS elemental analysis; Figure S2: Images of Fe_2O_3-NCs@SSM on EDS elemental analysis.; Figure S3: Images of OTS@Fe_2O_3-NCs@SSM on EDS elemental analysis; Table S1: Zeta potential values of the samples.

Author Contributions: Conceptualization, Y.S. and R.S.; methodology, Y.S.; validation, Z.K., C.S. and Q.W.; writing—original draft preparation, Y.S. and C.S.; writing—review and editing, Z.K., W.Y. and Z.Y. All authors have read and agreed to the published version of the manuscript.

Funding: This work was supported by Anhui Provincial Nature Science Research Program (KJHS-2019B07), Anhui Provincial Nature Science Research Project (2008085MH269), Anhui Provincial Teaching Team Project (2020jxtd250), and Huangshan University Talent Introduction Funding (2018xkjq005).

Institutional Review Board Statement: Not applicable.

Informed Consent Statement: Not applicable.

Data Availability Statement: The data presented in this study are available on request from the corresponding author.

Conflicts of Interest: The authors declare no conflict of interest.

References

1. Sam, E.K.; Liu, J.; Lv, X. Surface engineering materials of superhydrophobic sponges for oil/water separation: A review. *Ind. Eng. Chem. Res.* **2021**, *60*, 2353–2364. [CrossRef]
2. Luo, W.; Sun, D.; Chen, S.; Shanmugam, L.; Xiang, Y.; Yang, J. Robust microcapsules with durable superhydrophobicity and superoleophilicity for efficient oil-water separation. *ACS Appl. Mater. Interfaces* **2020**, *12*, 57547–57559. [CrossRef] [PubMed]
3. Liu, H.; Geng, B.; Chen, Y.; Wang, H. Review on the aerogel-type oil sorbents derived from nanocellulose. *ACS Sustain. Chem. Eng.* **2016**, *5*, 49–66. [CrossRef]
4. Elhenawy, S.; Khraisheh, M.; AlMomani, F.; Hassan, M.K.; Al-Ghouti, M.A.; Selvaraj, R. Recent developments and advancements in graphene-based technologies for oil spill cleanup and oil-water separation processes. *Nanomaterials* **2021**, *12*, 87. [CrossRef]
5. Yu, Z.L.; Li, G.C.; Fechler, N.; Yang, N.; Ma, Z.Y.; Wang, X.; Antonietti, M.; Yu, S.H. Polymerization under hypersaline conditions: A robust route to phenolic polymer-derived carbon aerogels. *Angew. Chem. Int. Ed.* **2016**, *55*, 14623–14627. [CrossRef]
6. Yang, Y.; Tong, Z.; Ngai, T.; Wang, C. Nitrogen-rich and fire-resistant carbon aerogels for the removal of oil contaminants from water. *ACS Appl. Mater. Interfaces* **2014**, *6*, 6351–6360. [CrossRef]
7. Bi, H.; Yin, Z.; Cao, X.; Xie, X.; Tan, C.; Huang, X.; Chen, B.; Chen, F.; Yang, Q.; Bu, X.; et al. Carbon fiber aerogel made from raw cotton: A novel, efficient and recyclable sorbent for oils and organic solvents. *Adv. Mater.* **2013**, *25*, 5916–5921. [CrossRef]
8. Bi, H.; Huang, X.; Wu, X.; Cao, X.; Tan, C.; Yin, Z.; Lu, X.; Sun, L.; Zhang, H. Carbon microbelt aerogel prepared by waste paper: An efficient and recyclable sorbent for oils and organic solvents. *Small* **2014**, *10*, 3544–3550. [CrossRef]
9. Zhang, M.; Xiao, C.; Zhang, C.; Qi, J.; Wang, C.; Sun, X.; Wang, L.; Xu, Q.; Li, J. Large-scale synthesis of biomass@MOF-derived porous carbon/cobalt nanofiber for environmental remediation by advanced oxidation processes. *ACS EST Eng.* **2020**, *1*, 249–260. [CrossRef]
10. Wen, H.; Hsu, Y.I.; Uyama, H. Superhydrophobic PDMS-pCA@CNWF composite with UV-resistant and self-cleaning properties for oil/water separation. *Materials* **2022**, *15*, 376. [CrossRef]
11. Tudu, B.K.; Sinhamahapatra, A.; Kumar, A. Surface modification of cotton fabric using TiO_2 nanoparticles for self-cleaning, oil-water separation, antistain, anti-water absorption, and antibacterial properties. *ACS Omega* **2020**, *5*, 7850–7860. [CrossRef]
12. Du, J.; Liu, L.; Hu, Z.; Yu, Y.; Zhang, Y.; Hou, S.; Chen, A. Raw-cotton-derived N-doped carbon fiber aerogel as an efficient electrode for electrochemical capacitors. *ACS Sustain. Chem. Eng.* **2018**, *6*, 4008–4015. [CrossRef]
13. Zhang, G.D.; Wu, Z.H.; Xia, Q.Q.; Qu, Y.X.; Pan, H.T.; Hu, W.J.; Zhao, L.; Cao, K.; Chen, E.Y.; Yuan, Z.; et al. Ultrafast flame-induced pyrolysis of poly(dimethylsiloxane) foam materials toward exceptional superhydrophobic surfaces and reliable mechanical robustness. *ACS Appl. Mater. Interfaces* **2021**, *13*, 23161–23172. [CrossRef]
14. Wu, F.; Pickett, K.; Panchal, A.; Liu, M.; Lvov, Y. Superhydrophobic polyurethane foam coated with polysiloxane-modified clay nanotubes for efficient and recyclable oil absorption. *ACS Appl. Mater. Interfaces* **2019**, *11*, 25445–25456. [CrossRef]
15. Ju, G.; Zhou, L.; Jiao, C.; Shen, J.; Luan, Y.; Zhao, X. One-step fabrication of a functionally integrated device based on polydimethylsiloxane-coated SiO_2 NPs for efficient and continuous oil absorption. *Materials* **2021**, *14*, 5998. [CrossRef]
16. Wang, J.; Fan, Z.; Liu, Q.; Tong, Q.; Wang, B. Fabrication of PDMS@Fe_3O_4/MS composite materials and its application for oil-water separation. *Materials* **2021**, *15*, 115. [CrossRef]
17. Panickar, R.; Sobhan, C.B.; Chakravorti, S. Highly efficient amorphous carbon sphere-based superhydrophobic and superoleophilic sponges for oil/water separation. *Langmuir* **2021**, *37*, 12501–12511. [CrossRef]
18. Liu, D.; Wang, S.; Wu, T.; Li, Y. A robust superhydrophobic polyurethane sponge loaded with multi-walled carbon nanotubes for efficient and selective oil-water separation. *Nanomaterials* **2021**, *11*, 3344. [CrossRef]
19. Han, S.; Song, Q.; Feng, X.; Wang, J.; Zhang, X.; Zhang, Y. Flame-retardant silanized boron nitride nanosheet-infused superhydrophobic sponges for oil/water separation. *ACS Appl. Nano Mater.* **2021**, *4*, 11809–11819. [CrossRef]
20. Zhou, B.; Bashir, B.H.; Liu, Y.; Zhang, B. Facile construction and fabrication of a superhydrophobic copper mesh for ultraefficient oil/water separation. *Ind. Eng. Chem. Res.* **2021**, *60*, 8139–8146. [CrossRef]
21. Liang, T.; Wang, B.; Fan, Z.; Liu, Q. Fabrication of superhydrophobic SA-CeO_2@Cu mesh and its application in oil-water separation. *ACS Omega* **2021**, *6*, 25323–25328. [CrossRef]
22. Kong, L.H.; Chen, X.H.; Yu, L.G.; Wu, Z.S.; Zhang, P.Y. Superhydrophobic cuprous oxide nanostructures on phosphor-copper meshes and their oil-water separation and oil spill cleanup. *ACS Appl. Mater. Interfaces* **2015**, *7*, 2616–2625. [CrossRef]
23. Yin, X.; He, Y.; Li, H.; Ma, X.; Zhou, L.; He, T.; Li, S. One-step in-situ fabrication of carbon nanotube/stainless steel mesh membrane with excellent anti-fouling properties for effective gravity-driven filtration of oil-in-water emulsions. *J. Colloid Interface Sci.* **2021**, *592*, 87–94. [CrossRef]
24. Wang, J.; Xu, J.; Chen, G.; Lian, Z.; Yu, H. Reversible wettability between underwater superoleophobicity and superhydrophobicity of stainless steel mesh for efficient oil-water separation. *ACS Omega* **2021**, *6*, 77–84. [CrossRef]
25. Song, J.; Liu, N.; Li, J.; Cao, Y.; Cao, H. Facile fabrication of highly hydrophobic onion-like candle soot-coated mesh for durable oil/water separation. *Nanomaterials* **2022**, *12*, 761. [CrossRef]
26. Avasthi, P.; Kumar, A.; Balakrishnan, V. Aligned CNT forests on stainless steel mesh for flexible supercapacitor electrode with high capacitance and power density. *ACS Appl. Nano Mater.* **2019**, *2*, 1484–1495. [CrossRef]
27. Wang, Z.; Kong, W.; Si, L.; Niu, J.; Liu, Y.; Yin, L.; Tian, Z. Robust and thermally stable butterfly-like $Co(OH)_2$/hexadecyltrimethoxysilane superhydrophobic mesh filters prepared by electrodeposition for highly efficient oil/water separation. *Ind. Eng. Chem. Res.* **2019**, *58*, 9576–9584. [CrossRef]

28. Raturi, P.; Yadav, K.; Singh, J.P. ZnO-nanowires-coated smart surface mesh with reversible wettability for efficient on-demand oil/water separation. *ACS Appl. Mater. Interfaces* **2017**, *9*, 6007–6013. [CrossRef]
29. Li, Y.; Liu, X.; Zhang, B. Durability and stability of superhydrophobic stainless steel mesh supported pure-silica zeolite beta coatings. *Ind. Eng. Chem. Res.* **2019**, *58*, 8044–8049. [CrossRef]
30. Yue, X.; Fu, D.; Zhang, T.; Yang, D.; Qiu, F. Superhydrophobic stainless-steel mesh with excellent electrothermal properties for efficient separation of highly viscous water-in-crude oil emulsions. *Ind. Eng. Chem. Res.* **2020**, *59*, 17918–17926. [CrossRef]
31. Feng, L.; Zhang, Z.; Mai, Z.; Ma, Y.; Liu, B.; Jiang, L.; Zhu, D. A super-hydrophobic and super-oleophilic coating mesh film for the separation of oil and water. *Angew. Chem. Int. Ed.* **2004**, *43*, 2012–2014. [CrossRef] [PubMed]
32. Chen, J.; Li, K.; Zhang, H.; Liu, J.; Wu, S.; Fan, Q.; Xue, H. Highly efficient and robust oil/water separation materials based on wire mesh coated by reduced graphene oxide. *Langmuir* **2017**, *33*, 9590–9597. [CrossRef] [PubMed]
33. Fu, C.; Gu, L.; Zeng, Z.; Xue, Q. One-step transformation of metal meshes to robust superhydrophobic and superoleophilic meshes for highly efficient oil spill cleanup and oil/water separation. *ACS Appl. Mater. Interfaces* **2020**, *12*, 1850–1857. [CrossRef] [PubMed]
34. Li, W.; Li, X.; Liu, J.; Zeng, M.J.; Feng, X.; Jia, X.; Yu, Z.Z. Coating of wood with Fe_2O_3-decorated carbon nanotubes by one-step combustion for efficient solar steam generation. *ACS Appl. Mater. Interfaces* **2021**, *13*, 22845–22854. [CrossRef]
35. Bae, S.H.; Karthikeyan, K.; Lee, Y.S.; Oh, I.K. Microwave self-assembly of 3D graphene-carbon nanotube-nickel nanostructure for high capacity anode material in lithium ion battery. *Carbon* **2013**, *64*, 527–536. [CrossRef]
36. Pham-Huu, C.; Vieira, R.; Louis, B.; Carvalho, A.; Amadou, J.; Dintzer, T.; Ledoux, M.J. About the octopus-like growth mechanism of carbon nanofibers over graphite supported nickel catalyst. *J. Catal.* **2006**, *240*, 194–202. [CrossRef]
37. Zhao, M.; Cao, K.; Liu, M.; Zhang, J.; Chen, R.; Zhang, Q.; Xia, Z. Dual-shelled $RbLi(Li_3SiO_4)_2$:$Eu^{(2+)}$ @Al_2O_3@ODTMS phosphor as a stable green emitter for high-power LED backlights. *Angew. Chem. Int. Ed.* **2020**, *59*, 12938–12943. [CrossRef]
38. Zhang, L.; Zhou, A.G.; Sun, B.R.; Chen, K.S.; Yu, H.Z. Functional and versatile superhydrophobic coatings via stoichiometric silanization. *Nat. Commun.* **2021**, *12*, 982. [CrossRef]
39. Han, S.; Yang, J.; Li, X.; Li, W.; Zhang, X.; Koratkar, N.; Yu, Z.Z. Flame synthesis of superhydrophilic carbon nanotubes/Ni foam decorated with Fe_2O_3 nanoparticles for water purification via solar steam generation. *ACS Appl. Mater. Interfaces* **2020**, *12*, 13229–13238. [CrossRef]
40. Friis, J.E.; Brons, K.; Salmi, Z.; Shimizu, K.; Subbiahdoss, G.; Holm, A.H.; Santos, O.; Pedersen, S.U.; Meyer, R.L.; Daasbjerg, K.; et al. Hydrophilic polymer brush layers on stainless steel using multilayered ATRP initiator layer. *ACS Appl. Mater. Interfaces* **2016**, *8*, 30616–30627. [CrossRef]
41. Qin, H.; Cao, H.; Zhao, Y.; Jin, G.; Cheng, M.; Wang, J.; Jiang, Y.; An, Z.; Zhang, X.; Liu, X. Antimicrobial and osteogenic properties of silver-ion-implanted stainless steel. *ACS Appl. Mater. Interfaces* **2015**, *7*, 10785–10794. [CrossRef]
42. Liu, Y.; Zhang, K.T.; Yao, W.G.; Zhang, C.C.; Han, Z.W.; Ren, L.Q. A facile electrodeposition process for the fabrication of superhydrophobic and superoleophilic copper mesh for efficient oil–water separation. *Ind. Eng. Chem. Res.* **2016**, *55*, 2704–2712. [CrossRef]
43. Cao, H.; Liu, Y. Facile design of a stable and inorganic underwater superoleophobic copper mesh modified by self-assembly sodium silicate and aluminum oxide for oil/water separation with high flux. *J. Colloid Interface Sci.* **2021**, *598*, 483–491. [CrossRef]
44. Gunatilake, U.B.; Bandara, J. Fabrication of highly hydrophilic filter using natural and hydrothermally treated mica nanoparticles for efficient waste oil-water separation. *J. Environ. Manag.* **2017**, *191*, 96–104. [CrossRef]
45. Gunatilake, U.B.; Bandara, J. Efficient removal of oil from oil contaminated water by superhydrophilic and underwater superoleophobic nano/micro structured TiO_2 nanofibers coated mesh. *Chemosphere* **2017**, *171*, 134–141. [CrossRef]
46. Ahlawat, S.; Singh, A.; Mukhopadhyay, P.K.; Singh, R.; Bindra, K.S. Nanosecond laser induced glass particle deposition over steel mesh for long-term superhydrophilicity and gravity driven oil water separation. *Mater. Chem. Phys.* **2021**, *263*, 124343. [CrossRef]